Applied Radiation and Isotopes 107 (2016) 152–159

Contents lists available at ScienceDirect

Applied Radiation and Isotopes

journal homepage: www.elsevier.com/locate/apradiso

Semi-empirical model for fluorescence lines evaluation in diagnostic x-ray beams

Marco Bontempi [a,b,*], Lucia Andreani [c,d], Claudio Labanti [d,e], Paulo Roberto Costa [f], Pier Luca Rossi [c], Giuseppe Baldazzi [c,d]

[a] Laboratorio NaBi (Nano-Biotecnologie), Istituto Ortopedico Rizzoli, via di Barbiano 1/10, I-40136 Bologna, Italy
[b] Laboratorio di Biomeccanica ed Innovazione Tecnologica, Istituto Ortopedico Rizzoli, via di Barbiano 1/10, I-40136 Bologna, Italy
[c] Department of Physics, University of Bologna, viale Berti Pichat 6/2, I-40127 Bologna, Italy
[d] INFN Bologna, viale Berti Pichat 6/2, I-40127 Bologna, Italy
[e] INAF - IASF, via P. Gobetti 101, I-40129 Bologna, Italy
[f] Institute of Physics, University of São Paulo, Rua do Matao, travessa R, 187 Cidade Universitaria, São Paulo, Brazil

HIGHLIGHTS

- A semi-empirical model of fluorescence lines evaluation is proposed.
- Indirect radiation interaction is discussed.
- A semi-model of direct radiation interaction is presented and described.
- Experimental tests are presented and used to calibrate the model parameters.
- A comparison with independent data taken from the literature is discussed.

ARTICLE INFO

Article history:
Received 9 May 2014
Received in revised form
14 October 2015
Accepted 15 October 2015
Available online 23 October 2015

PACS:
87.64.Aa
29.30.Kv
32.80.Aa
89.20.Bb

Keywords:
x-ray
Bremsstrahlung
Fluorescence lines
Direct radiation
Indirect radiation

ABSTRACT

Diagnostic x-ray beams are composed of bremsstrahlung and discrete fluorescence lines. The aim of this study is the development of an efficient model for the evaluation of the fluorescence lines. The most important electron ionization models are analyzed and implemented. The model results were compared with experimental data and with other independent spectra presented in the literature. The implemented peak models allow the discrimination between direct and indirect radiation emitted from tungsten anodes. The comparison with the independent literature spectra indicated a good agreement.

1. Introduction

Since its discovery, the x-radiation became a very useful tool. Several imaging applications, such as conventional and interventionist radiology, computed tomography and mammography, use x-ray polychromatic beams composed of a bremsstrahlung continuous component together with fluorescence lines.

Many attempts for computing theoretical x-ray spectrum were developed and enhanced over time. However, few rigorous calculation method was developed to evaluate the characteristic radiation, possibly due to its relatively small contribution (10–15%) in comparison with the bremsstrahlung component (Birch and Marshall, 1979; Tucker et al., 1991; Poludniowski, 2007). Indeed, the three mathematical models more consistently validated for diagnostic x-ray spectra calculations are focused on the

* Corresponding author at: Laboratorio NaBi (Nano-Biotecnologie), Istituto Ortopedico Rizzoli, via di Barbiano 1/10, I-40136 Bologna, Italy. Fax: +39 051 583789.
E-mail address: m.bontempi@biomec.ior.it (M. Bontempi).

http://dx.doi.org/10.1016/j.apradiso.2015.10.018
0969-8043/

bremsstrahlung and only provide a rough description of characteristic radiation in terms of completeness (Birch and Marshall, 1979; Tucker et al., 1991; Poludniowski and Evans, 2007; Poludniowski, 2007).

Poludniowski (2007) described the x-ray spectrum and developed a calculation of the characteristic radiation that was based on a semi-empirical description of the *indirect* radiation component for tungsten anodes.

The model developed by Birch and Marshall (1979) is considered accurate and the faster model for simulating x-ray spectrum via Monte Carlo algorithms (Bontempi et al., 2010). It uses the Green and Cosslett (1968) empirical model to describe tungsten characteristic radiation as a function of the tube voltage. Birch and Marshall also used the Storm and Israel (1970) Data Tables to calculate the energies and the relative intensities of K and L fluorescence lines. The other model, developed by Tucker et al. (1991), modified by Costa et al. (2007), uses the same empirical description adjusting the exponent value (1.67 as opposed to 1.63) according to Green and Cosslett (1961) theoretical predictions. It then incorporates the terms studied by Vignes and Dez (1968) to take into account the depth of production of the characteristic x-rays. Pella et al. (1985) implemented an algorithm to evaluate the fluorescence lines of various materials starting from the work of Green and Cosslett (1961) and calculating the ratio between characteristic radiation and bremsstrahlung continuum component.

Although the peak models discussed treat both the direct and indirect radiations, their formulations are based on a very old x-ray model (Kramers, 1923) that has many approximations and strong hypotheses that make it unusable for calculating real x-ray spectra.

Moreover, the direct characteristic radiation description proposed by Green and Cosslett (1961) is derived from the non-relativistic ionization cross section of Bethe (1930). So the presented models are based on approximations. They are valid but old, and sometimes obsolete.

Thus the aim of this work is to analyze the contribution of fluorescent radiation using modern direct and indirect radiation models. Three major models of electron ionization cross section will be analyzed and implemented and the most effective and accurate will be chosen and used to simulate x-ray characteristic radiation.

2. Materials and methods

The description of direct and indirect characteristic radiation starts from the observation of the physical phenomena that happen inside the x-ray tube. There are three major events that can happen: electron ionization (*direct radiation*), Auger electron emission (negligible, Dyson, 1990) and photoelectric ionization and vacancy fill (*indirect radiation*). Together with the bremsstrahlung photon production, these phenomena contribute to make the x-ray spectrum:

$$n_{sp}(E) = Qf(E)\left(n_{br}(E) + \sum_j \delta(E - E_j)n_j\right) \tag{1}$$

where Q takes into account the source–detector distance, the beam collimation, the tube current, the exposure time and the detection efficiency. The term $f(E)$ indicates the total filtration of the x-ray tube (housing/inherent plus additional filtration) and depends on the photon energies. The functions n_{br} and n_j refer to the counts of bremsstrahlung and characteristic photons. The Dirac delta function, $\delta(E - E_j)$, selects the peak position in terms of the energy to be added to the bremsstrahlung continuum. In an experimental spectrum, the δ appears as a bell-shaped peak that depends on the energy resolution of the instruments used for detecting the spectra.

In order to clarify the notations used, the symbol "E" refers to photon energy, "T" is used to indicate the electron kinetic energy and "kVp" indicates the value of the x-ray tube voltage. The subscript "k" then refers to the k-th atomic shell (K, L, M, N) with energy E_k while the subscript "j" refers to the j-th characteristic peak (es: $K_{\alpha 1}$, or $K_{\alpha 2}$, etc.) with centroid energy E_j.

2.1. Indirect radiation

One of the most robust models for accounting the production of the *indirect* characteristic radiation was proposed by Poludniowski (2007).

The amount of characteristic photons was evaluated considering that the ratio of direct and indirect radiation is constant over a wide range of tube voltages, as stated by Dyson (1990). According to the Poludniowski model, the intensity of the indirect radiation is

$$n_j^{ind} = p_j f_j A_k N_{br}^{emit} \tag{2}$$

where p_j is the intensity of the j-th peak (Thompson et al., 2009), f_j is the total filtration of the tube at the j-th peak energy, and A_k is the probability that a bremsstrahlung photon will appear as indirect radiation (Poludniowski, 2007). ${N_{br}}^{emit}$ is the total number of bremsstrahlung photons emitted with energies $E \geq E_k$:

$$N_{br}^{emit} = Q\int_{E_k}^{kVp} n_{br}(E)\,dE \tag{3}$$

Then Poludniowski described the contribution of the term A_k, reaching the final formulation of the total characteristic radiation:

$$n_j = (1 + p_d)n_j^{ind} \tag{4}$$

where p_d is the ratio between direct and indirect radiation.

2.2. Direct radiation

As previously stated, the other component of the characteristic radiation is the direct interaction of the cathode-emitted electrons with the orbital electrons into the anode material. This interaction could ionize the anode atoms and generate photons with a well-defined energy.

The model of Green and Cosslett (1961) was based on the equation

$$n_k^{dir} = \frac{\rho N_A}{A} Q\int_{E_k}^{kVp} \sigma_k(T)\left(\frac{dT}{dx}\right)^{-1} dT \tag{5}$$

where $\frac{\rho N_A}{A}$ is the number of atoms per volume unit in the target, ρ is the density of the target, N_A is Avogadro's number, A is the atomic weight of the target and σ_k is the ionization cross section at the k-th shell and $\frac{dT}{dx}$ is the electron stopping power inside the anode. This equation does not take into account the auto-absorption of the generated photons inside the anode and the parameter σ_k was based on the Bethe (1930) non-relativistic electron-ionization cross section.

On the basis of the models of Birch and Marshall (1979) and Tucker et al. (1991), this equation can be updated adding the auto-absorption of the anode. Thus the final form of the direct characteristic radiation is

$$n_j^{dir} = Qf_j p_j B_k\left[\frac{\rho N_A}{A}\int_{E_k}^{kVp} \sigma_k(T)e^{-\mu_j d_T}\left(\frac{dT}{dx}\right)^{-1} dT\right] \tag{6}$$

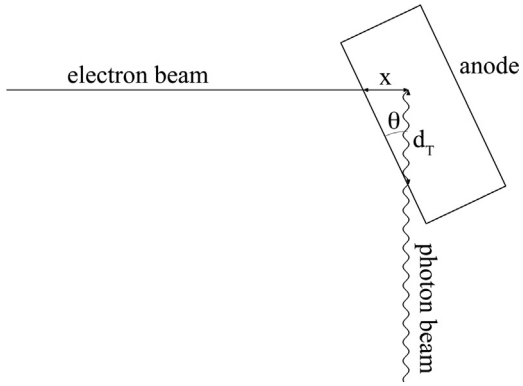

Fig. 1. Scheme of the electron and photon paths inside the anode. The x variable is the distance of the electron inside the anode, while d_T indicates the distance travelled by photons to emerge from the anode. θ represents the anode slope with respect to the x-ray beam axis.

where μ_j is the linear attenuation coefficient of the anode material calculated at energy E_j. The term B_k is the probability that an ionization event will produce a direct radiation photon and it is strictly dependent on the ionization cross section models. Since the integration approach used is an approximation, the parameter B_k takes into account all the stochastic phenomena that are involved in the photon production process, including secondary scattering of electrons and multiple scattering events leading to energy straggling.

The term d_T is the distance between the generation point of the photon to the anode exit surface (Fig. 1). The bremsstrahlung models presented in the literature use the Thomson–Whiddington equation (Birch and Marshall, 1979) to correlate electron depth with energy. According to the geometries used in this work, the term d_T can be expressed as $d_T = x \cot\theta$, where θ is the anode angle and x is the electron depth evaluated using the Thomson–Whiddington relationship. A more general formulation of this equation was presented in Bontempi et al. (2010).

Thus the number of characteristic photons is

$$n_j = (1 + p_i) n_j^{dir} \tag{7}$$

where p_i is the ratio between the contributions of indirect and direct radiation.

2.3. Electron ionization cross section

To proceed with the evaluation of the number of produced photons, it is necessary to choose the appropriate ionization cross section.

Some theoretical (Gryzinski, 1965a), semi-empirical (Deutsch et al., 2000) and empirical models (Casnati et al., 1982; Hombourger, 1998; Talukder et al., 2008; Tang et al., 2001) have been proposed to evaluate the cross section for the atomic shell vacancies produced by electron impact. Most of them describe the total ionization cross-section referred to as a thin target, so it is necessary to extend these models to thick anodes.

Casnati et al. (1982) proposed an empirical model that describes the ionization cross section of atomic K-shell by electron impact and fits experimental data and theoretical results in the ranges of $6 \le Z \le 79$ and $1 \le T/E_k \le 20$.

An evolution of that model was developed by Hombourger (1998). This is also an empirical model that describes the K-shell ionization cross sections by electron impact, with a wide range of validity: $6 \le Z \le 79$ and $1 \le T/E_k \le 10^4$.

Empirical models have simple algorithms, but these are approximations and therefore have limited validity. Nonetheless, the two models outlined above are perfectly usable in the range of application involved in this work.

In order to conduct a complete evaluation of the approaches presented in the literature, theoretical models were also considered. A major theoretical model was developed by Gryzinski (1965a). It was a classical attempt to describe the ionizations of atoms by electrons, based on Coulomb scattering and related parameters to describe the target system. The model is based on a relatively simple analytical formula of the cross section which can be completed with a relativistic correction factor for high energies of the incident electron (Gryzinski, 1965b) and can be applied to all shells. Although L lines are not relevant for applications in diagnostic imaging due to their low-energies, the Gryzinski model can be used to obtain them.

2.4. Radiation contribution evaluations

The contribution of direct/indirect radiation, and the associated parameters (A_k, B_k, p_i and p_d), can be evaluated through a series of experimentally acquired spectra. As previously described, the experimental spectra are affected by filtration and setup parameters ($f(E)$ and Q) and have to be corrected before using them. It is particularly necessary to compensate the contribution of the total filtration $f(E)$. This can be accomplished by dividing Eqs. (1)–(3) and (6) by $f(E)$, or f_j. This mathematical correction might be critical in energies beyond the k-edge of low photon fluence spectra, where the Signal-to-Noise-Ratio could be low. While this is true, the correction at these energy intervals is so minimal that possible errors can be ignored. Nevertheless, this correction is required to obtain more reliable results.

Since the desired parameters are not a function of the photon energy, it is more useful to work with the total value of the characteristic photons than with individual peaks. In this way the sum of the contributions of all peak photons eliminates the dependence on "j" and maintains only the dependence on "k". Consequently, the total number of photons will be indicated as

$$N_k = \sum_j \frac{n_j}{f_j} \tag{8}$$

where n_j was defined using Eqs. (2), (4) (or 6), (7) and with the fact that $\sum p_j = 1$. With this definition, it is possible to calculate the value of the parameters:

$$(1 + p_d) A_k = \frac{N_k}{N_{br}^{emit}}$$

and this result does not depend on the experimental setup (Q). As the evaluation of the term A_k is fully described by Poludniowski, it is possible to evaluate p_d and consequently p_i:

$$\begin{cases} p_d = \dfrac{1}{A_k} \dfrac{N_k}{N_{br}^{emit}} - 1 \\ p_i = \dfrac{1}{p_d} \end{cases} \tag{9}$$

The direct radiation contribution is determined from these quantities.

The last step is to evaluate the term B_k in Eq. (6). To simplify the notation and the calculation, it is useful to define

$$N_k^{ion} = \frac{\rho N_A}{A} \sum_j \left[p_j \int_{E_k}^{kVp} \sigma_k(T) e^{-\mu_j d_T} \left(\frac{dT}{dx} \right)^{-1} dT \right] \tag{10}$$

Combining Eqs. (6)–(8) and (10), the term QB_k became

$$QB_k = \frac{N_k}{(1 + p_i) N_k^{ion}} \tag{11}$$

Table 1
List of the experimental setup parameters used for the spectra acquisitions.

Tube	MHF160
Generator	CHF 225 kV, 1.6 kW
Manufacturer	Gilardoni Spa, Mandello del Lario (LC), Italy
Anode angle	20°
Anode material	Tungsten (W)
Total filtration	0.8 mmBe
Nominal focal spot size	0.4 mm
Current	1 mA
Emission time	620 s
Voltage used (kV)	90, 100, 110, 120, 130, 140, 150
Detector	GLP-10180/07-P
Manufacturer	Ortec, Oak Ridge (TN), USA
Preamplifier	7611 Spectroscopy Amplifier
Manufacturer	Silena spa, Rome (RM), Italy
MCA model	MCS8000A, 1024 channels
Software	ADMCA v2.0.0.5
Manufacturer	Amptek Inc, Bedford (MA), USA
Live time	600 s
Dead time	<1%
Source-detector distance	(558 ± 2) cm air
Beam collimation	(0.8 ± 0.1) cm^2 at detector surface

Thus the correct value of QB_k can be operatively evaluated by means of a linear fitting of N_k as a function of $(1 + p_i)N_k^{ion}$ for every tube voltage.

The term Q cannot be determined and remains an empirical parameter due to the lack of available data. Therefore B_k cannot be fully evaluated. Because it is a probability, it must be presented as $B_k \leq 1$, so $Q \geq \frac{1}{(QB_k)}$. As Q is independent of the cross section models, the highest of the QB_k values was used to evaluate it.

2.5. Experimental tests

The characteristic radiation models were evaluated with respect to their efficiency and degree of agreement with experimental data.

Models were experimentally calibrated by acquiring a reference set of spectra from a conventional x-ray tube and evaluating the measured peak areas. The source, detector and geometrical parameters used in this experiment are listed in Table 1. The HPGe detector used to acquire the spectra was calibrated using gamma lines of ^{241}Am and ^{57}Co. To optimize the photon collection efficiency, the two sources were positioned on the detector input surface. The photo-peaks were acquired and the Full-Width-at-Half-Maximum (FWHM) of each peak was used to determine the detector energy resolution. After the energy calibration, the detection beamline was set as showed in Fig. 2.

In order to avoid adjustments of the voltage/current ripple, the beam was active for a duration of 620 s. The detection started 10 s after the beam activation and ended 10 s before the deactivation. An additional interval of 30 s passed between two subsequent measurements in order to avoid any potential spectra modification due to anode temperature effects. The acquired spectra were then corrected by detector energy efficiency.

The first test on the experimental spectra concerned the determination of the direct and indirect radiation contributions, described in the previous section, as well as evaluating the Q, A_k, B_k, p_d and p_i parameters.

Once the parameters p_d and p_i were estimated, the contribution of the direct and indirect radiation were evaluated, from Eqs. (4), (7), and (8) and the experimental data, as

$$\begin{cases} N_{k-ind} = \dfrac{1}{1+p_d} N_k \\ N_{k-dir} = \dfrac{1}{1+p_i} N_k \end{cases} \tag{12}$$

The direct radiation (Eq. (6)) was then used to test the power of the model to predict the peak areas. Then the uncertainties of the results were estimated evaluating the fit parameters using the least-square-method and applying the error propagation to the model equations.

After the evaluation of the model parameters, a C++ simulation, based on Bontempi et al. (2010), was implemented to replicate the experimental spectra. Each cross section model and the direct radiation photon emission (Eqs. (6) and (7)) were inserted inside the software and all the experimental protocols were duplicated and compared with the real spectra.

The model accuracy was tested comparing the measured net area of the experimental peaks with the corresponding values provided by the models, sampled at 1 keV. The experimental peak areas were extracted from the spectra using a peak identification function written in MATLAB (ver. 2011a, The Mathworks Inc., Natick, MA, USA) and the bremsstrahlung continuum was subtracted implementing the baseline correction algorithm described in Gan et al. (2006). Then, the peaks were extracted applying a threshold to the remaining counts.

The comparison was carried out using the Root Mean Square Deviation (RMSD) defined as

$$RMSD = \sqrt{\frac{1}{n}\sum_{j=1}^{n}\left(n_j^{cal} - n_j^{exp}\right)^2} \tag{13}$$

where n is the number of peaks, c_j^{cal} is the calculated area and n_j^{exp} is the experimental area of the j-th peak. The model with the lowest RMSD value was identified as the most accurate.

Following the model calibration, the proposed model was

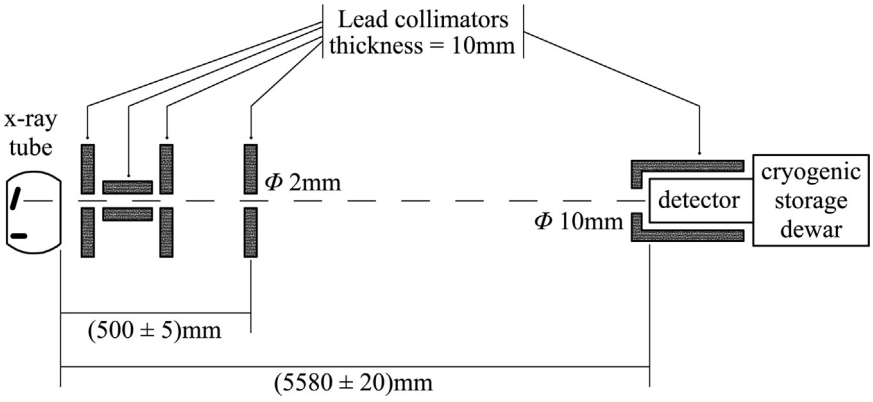

Fig. 2. Scheme of the collimation geometry used in the experimental spectrometry.

tested comparing the calculated K-characteristic lines with the spectrum models discussed in the introduction (Birch and Marshall, 1979; Tucker et al., 1991; Poludniowski, 2007) and with the independent data presented in the literature (Fewell and Shuping, 1977; Fewell et al., 1981; Bhat and Pattison, 1998). The data provided by these articles are organized in terms of bremsstrahlung and characteristic peaks, so it is possible for a direct comparison between their results and the proposed calculations. Then the calculated and the experimental spectra from Fewell et al. and Bhat and Pattison were compared according to their peak areas with the models. The energy resolution of the calculations was adapted to the experimental spectra in order to get a direct comparison. The peak areas were compared by calculating the residuals between the experimental peak data and the considered models: present (SIM), Birch and Marshal (BM), Tucker et al. (TBC) and Poludniowski (PDK). Because the calculated residuals are independent random variables, the overall comparison was evaluated as the average of all the residuals and this was used as a quantification of the accuracy of the models.

3. Results

Table 2 shows the results of the HPGe detector energy calibration. The experimental energy resolution was thus set to the upper limit of the FWHM, i.e. 0.5 keV.

Fig. 3 shows the measured spectra.

After the calibration, the model parameters are evaluated, according to Eqs. (9)–(11).

Table 3 lists the peak areas measured through experiments.

Table 4 lists the unfiltered peak areas and their sums. The attenuation coefficients used were taken from the NIST database (Hubbell and Seltzer, 1996). The comparison between Tables 3 and 4 shows that, although there is a significative difference between experimental and unfiltered data (about 14%), no remarkable instabilities can be highlighted. This is in accordance with what was assumed in Section 2.4.

Fig. 4 shows the correlation between the number of photons with energy $E > 69.52$ keV (the K-edge of tungsten) and the number of photons emitted as K-peaks. The figure shows an excellent linear correlation ($R^2 = 0.997$). This validates both the statement proposed by Dyson (1990) and the model developed by Poludniowski (2007) and confirms that the ratio between direct and indirect radiation is constant, at least, over the voltage range considered in this study. On the basis of these results, and using the value of $A_k = 0.36$ for K-edge tungsten as established by Poludniowski, it is possible to assess the values of p_d and p_i as showed in Table 5. The calculated value of p_d and p_i is then used to estimate the number of peak photons of direct and indirect radiation using Eq. (12), showed in Table 6 and Fig. 5.

The last parameter to evaluate is B_k, i.e. the probability that an ionization event will generate a characteristic photon. Table 7 shows the evaluations of the integral in Eq. (11) according to the different considered cross section models. Fig. 6 shows the trend for N_k as a function of $(1 + p_i)N_k^{ion}$. The figure also shows the best-fit line for each of the three cross section models. Although the three models show a slight curvature, it is so minimal that the linear fit can be considered an excellent approximation for the range of voltages considered in this work. This is also quantitatively justified by the fact that the linear correlation coefficients of the fits are 0.9969 for Gryzinsky, 0.9984 for Casnati and 0.9974 for Hombourger.

For each model, the results of the data linear fitting (Fig. 6) are showed in Table 8.

The RMSD (Eq. (13)) between the calculated peak areas and the

Table 2
Results of the HPGe detector energy calibration. The table indicates the photo-peak energy centroids for each used element and the FWHM of the detected photo-peak.

Source	Peak centroid energy (keV)	FWHM (keV)
^{241}Am	26.34	0.270
^{241}Am	59.54	0.360
^{57}Co	122.00	0.480

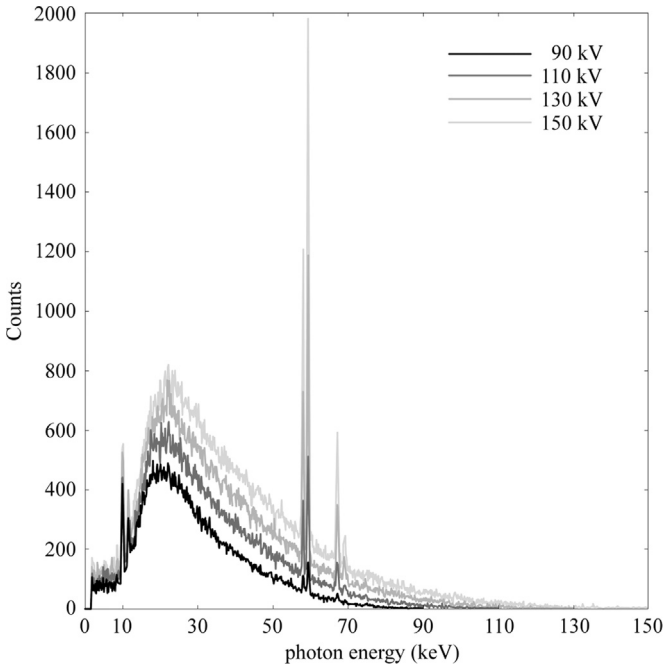

Fig. 3. Plot of a sample of the experimentally measured spectra. Only the spectra at 90, 110, 130 and 150 kVp are showed.

Table 3
Results of the experimentally measured peak areas (n_j) for each used tube tension. The columns show the corresponding peak centroid energy in keV.

kVp	$(E_j \pm 0.5)$ keV			
	58.0	59.5	67.0	69.0
90	193	339	112	–
100	306	695	279	90
110	663	1328	264	193
120	1091	2065	690	163
130	1687	3092	909	126
140	2335	4159	1366	399
150	2903	5449	1725	209

Table 4
Unfiltered experimental peak areas (n_j/f_j). The last two columns report the total number of peak photons (N_k) and the total back-filtered photons emitted with energy $E > 69.52$ keV (N_{br}^{emit}).

kVp	$(E_j \pm 0.5)$ keV				N_k	N_{br}^{emit}
	58.0	59.5	67.0	69.0		
90	221	388	127	–	736	1061
100	351	795	317	102	1565	2526
110	760	1520	300	219	2799	4962
120	1251	2364	784	185	4583	8370
130	1934	3539	1033	143	6649	12,243
140	2677	4760	1552	53	9442	16,607
150	3328	6236	1960	237	11,762	22,102

For each model, the results of the data linear fitting (Fig. 6) are showed in Table 8.

The RMSD (Eq. (13)) between the calculated peak areas and the

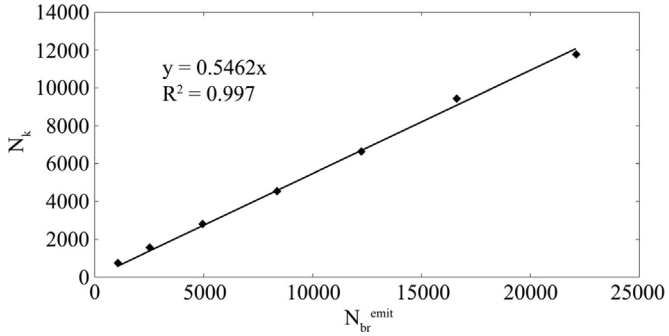

Fig. 4. Plot of the number of photons with $T > 69.52$ keV (N_{br}^{emit}) and the N_k.

Table 5
Values estimated for $(1 + p_d)A_k$, p_d and p_i.

$(1 + p_d)A_k$	p_d	p_i
0.546 ± 0.007	0.50 ± 0.02	1.98 ± 0.08

Table 6
Number of direct (N_{k-dir}) and indirect radiation (N_{k-ind}) as a function of the tube voltage estimated using equations (7) and (4) and the parameters estimated for p_d and p_i.

kVp	$N_{k-dir} \pm 4\%$	$N_{k-ind} \pm 4\%$
90	247	490
100	524	1040
110	938	1860
120	1540	3050
130	2230	4420
140	3160	6280
150	3940	7820

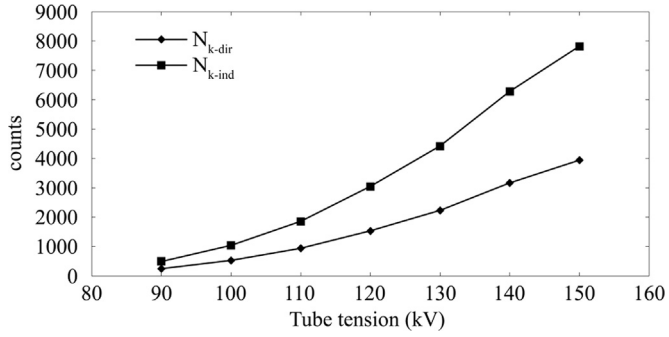

Fig. 5. Plot of the direct and indirect radiations as a function of the tube voltage.

Table 7
Values of $N_k^{ion} \times 10^{-4}$ (Eq. (10)) per incident electron as a function of the tube voltage for each model.

kVp	Gryzinski	Casnati et al.	Hombourger
90	1.24	1.10	1.98
100	3.27	2.45	4.39
110	6.44	4.28	7.68
120	10.82	6.53	11.77
130	16.39	9.11	16.56
140	23.10	11.96	21.93
150	30.88	15.01	27.80

experimental data at each tube voltage are showed in Table 9.

By the observation of Table 9, it is clear that the Homburger model is the most accurate, followed by Casnati et al. and Gryzinski. For this reason the Hombourger model was chosen for

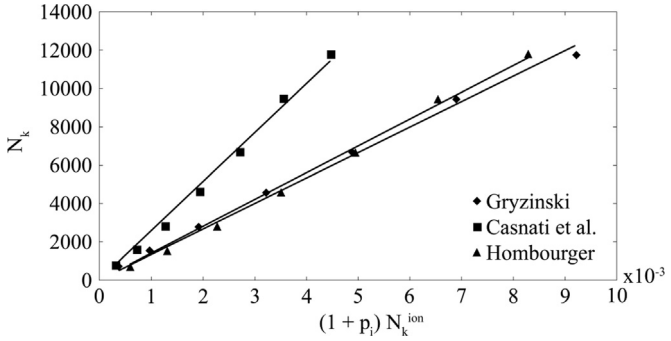

Fig. 6. Plot of N_k as a function of $(1 + p_i)N_k^{ion}$.

Table 8
Values of QB_k evaluated by fitting N_k and $(1 + p_i)N_k^{ion}$ for each cross section model as described in Eq. (11) and estimations of the parameters Q and B_k.

	Gryzinski	Casnati et al.	Hombourger
$QB_k \pm 2\%$	$1.33 \cdot 10^6$	$2.56 \cdot 10^6$	$1.39 \cdot 10^6$
$Q \geq 2.56 \cdot 10^6 \pm 2\%$			
$B_k \leq$	$0.52 \pm 4\%$	$1.00 \pm 4\%$	$0.55 \pm 4\%$

Table 9
Models RMSD results at different tube voltages and total average.

kVp	Gryzinsky	Casnati et al.	Hombourger
90	87	16	13
100	83	98	91
110	119	128	116
120	111	92	79
130	130	44	47
140	100	115	108
150	112	238	205
Average	99	86	79

Table 10
Comparison of the calculated peak areas using the Hombourger model in Eq. (6) (SIM) and the other spectrum models of the literature: BM (Birch and Marshall, 1979), TBC (Tucker et al., 1991), PDK (Poludniowski, 2007). The keV column lists the energies associated to each peak.

	keV	SIM ± 2%	BM	TBC	PDK
			$\times 10^{-3}$		
80 kVp	60	9.4	9.544	13.36	13.45
	68	2.00	1.681	2.99	2.748
	70	0.484	0.00268	0.412	0.3876
100 kVp	60	26.8	37.22	106.8	42.81
	68	5.5	8.101	24.64	9.298
	70	1.31	0.682	5.238	1.641

Table 11
Comparison of the experimental peak areas and calculations using the Hombourger model in equation (6). The keV column lists the energies associated to each peak.

	keV	SIM ± 2%	Fewell et al.	Bhat–Pattison
			$\times 10^{-3}$	
80 kVp	60	9.4	9.569	11.779
	68	2.00	1.940	3.018
	70	0.484	0.360	0.610
100 kVp	60	26.8	23.262	29.064
	68	5.5	8.519	10.754
	70	1.31	2.946	1.854

Table 12
Residuals between the peak areas calculated with the indicated models and the data from Fewell and Shuping (1977). The keV column lists the energies associated to each peak.

	keV	Fewell-SIM	Fewell-BM	Fewell-TBC	Fewell-PDK
80 kVp	60	$3.42{\cdot}10^{-8}$	$6.62{\cdot}10^{-10}$	$1.44{\cdot}10^{-5}$	$1.51{\cdot}10^{-5}$
	68	$3.84{\cdot}10^{-9}$	$6.71{\cdot}10^{-8}$	$1.10{\cdot}10^{-6}$	$6.53{\cdot}10^{-7}$
	70	$1.53{\cdot}10^{-8}$	$1.28{\cdot}10^{-7}$	$2.70{\cdot}10^{-9}$	$7.62{\cdot}10^{-9}$
100 kVp	60	$1.22{\cdot}10^{-5}$	$1.95{\cdot}10^{-4}$	$6.98{\cdot}10^{-3}$	$3.82{\cdot}10^{-4}$
	68	$9.11{\cdot}10^{-6}$	$1.75{\cdot}10^{-7}$	$2.60{\cdot}10^{-4}$	$6.07{\cdot}10^{-7}$
	70	$2.68{\cdot}10^{-6}$	$5.13{\cdot}10^{-6}$	$5.25{\cdot}10^{-6}$	$1.70{\cdot}10^{-6}$
	average	$4.01{\cdot}10^{-6}$	$3.34{\cdot}10^{-5}$	$1.21{\cdot}10^{-3}$	$6.67{\cdot}10^{-5}$

Table 13
Residuals between the peak areas calculated with the indicated models and the data from Bhat and Pattison (1998). The keV column lists the energies associated to each peak.

	keV	Bhat-SIM	Bhat-BM	Bhat-TBC	Bhat-PDK
80 kVp	60	$5.74{\cdot}10^{-6}$	$4.99{\cdot}10^{-6}$	$2.50{\cdot}10^{-6}$	$2.79{\cdot}10^{-6}$
	68	$1.03{\cdot}10^{-6}$	$1.79{\cdot}10^{-6}$	$7.84{\cdot}10^{-10}$	$7.29{\cdot}10^{-8}$
	70	$1.59{\cdot}10^{-8}$	$3.69{\cdot}10^{-7}$	$3.92{\cdot}10^{-8}$	$4.95{\cdot}10^{-8}$
100 kVp	60	$5.31{\cdot}10^{-6}$	$6.65{\cdot}10^{-5}$	$6.04{\cdot}10^{-3}$	$1.89{\cdot}10^{-4}$
	68	$2.76{\cdot}10^{-5}$	$7.04{\cdot}10^{-6}$	$1.93{\cdot}10^{-4}$	$2.12{\cdot}10^{-6}$
	70	$2.97{\cdot}10^{-7}$	$1.37{\cdot}10^{-6}$	$1.15{\cdot}10^{-5}$	$4.54{\cdot}10^{-8}$
	Average	$6.67{\cdot}10^{-6}$	$1.37{\cdot}10^{-5}$	$1.04{\cdot}10^{-3}$	$3.23{\cdot}10^{-5}$

evaluating the direct radiation with Eq. (6) and the K-peak lines using Eq. (7).

The last test concerned the comparison of the spectra described in the literature and the model of K-lines generated using the Hombourger model (SIM) and the models presented by Birch and Marshall (1979) (BM), Tucker et al. (1991) (TBC) and Poludniowski (2007) (PDK) are showed in Table 10. The comparison of the present model with the peaks evaluated by Fewell and Shuping (1977) and by Bhat and Pattison (1998) are showed in Table 11.

The accuracy of the models with respect to the experimental data from the literature is showed in Tables 12 and 13. The last row of the two tables shows the average residual value. It is clear that the presented model (SIM) has the lowest discrepancy from the experimental.

4. Discussion

The presented results provide information about the behavior of direct and indirect radiation emerging from the anode of an x-ray tube. The parameters required to describe the peaks were evaluated considering the data from the literature and the experimental tests. In this way a detailed description of the direct and indirect radiation has been showed (Table 6 and Fig. 5).

Fig. 4 clearly indicated that the experimental data are in excellent agreement with the linear correlation proposed by Poludniowski and Dyson and represented in Eq. (2). This allows us to evaluate the parameter p_d with a great accuracy (4%). Other models treated this parameter as empirically determined and dependent on the experimental conditions. In this case, instead, the value is independent from the experimental conditions and is related to the anode material. According to these evaluations the contribution of the direct and indirect radiation was determined. Table 6 and Fig. 5 show that the contribution of direct radiation to the K-peaks is much lower than the indirect, according to Green and Cosslett (1961) and Tothill (1968) results. The results of the partition between direct and indirect radiation were then used to evaluate the performances of each cross section models and to evaluate the parameter QB_k. Fig. 6 shows an excellent agreement in the 90–150 kV range between the considered data and the calculated photon production by ionization using Eq. (10) with a correlation coefficient very close to 1. This is a justification of the hypothesis of linearity between the number of ionization and direct radiation through B_k, as outlined in Eq. (6). It also represents a corroboration of the parameter Q meaning. Both these parameters are independent from the peak energies (E_j), while B_k depends only on the atomic number (Z) and the edge energy (E_k) of the anode material. Similarly, Q depends exclusively on the experimental parameters and setup. Although these parameters are very important, it was not possible to split their contributions using the available data, nor from the experimental tests, neither from the literature data. The only determination, which could be made, was limiting estimations of the allowed values as showed in Table 8. The parameter Q has a very large lower-limit, which can be explained by looking at its meaning: it depends on the geometrical setup and contains data about the total number of electrons impacting the anode (600 mA s represents a very large number of electrons). The fact that $B_k \leq 1$ can be explained by considering the photons produced through the ionization process. There are two main modes of interactions: decay from outer shells, and interaction with free electrons. The first phenomenon is what is commonly accepted as direct characteristic line (Dyson, 1990; Thompson et al., 2009). However not every ionization is followed by a decay from the outer shells, but a recombination with free electrons can also occur. This recombination refers to the second mode of interaction. Not all the free electrons have a probability to fill a ionization hole, in fact, only those electrons with an energy lower than E_k can do this. Moreover not all the produced photons have enough energy to emerge from the anode. This fact reduces the probability that every ionization will produce a K-photon which will emerge from the anode, and so $B_k < 1$. After calibrating the direct radiation models, a final test was performed to choose the best cross section model. As can be seen in Table 9 the Hombourger model was selected as the most accurate. This is not surprising since it is the most recently introduced model and takes into account the correction required to modify the Gryzinski and Casnati models. Therefore the measurements in this work confirm also what was stated by Hombourger and validate his model.

The comparison of the peaks calculated with the model presented here (SIM), with the other proposed models (BM, TBC, PDK) and with the experimental (Fewell et al. and Bhat and Pattison) shows that the presented model is in general the most accurate, as showed in Tables 12 and 13 where the mean residual of the present work (SIM) with respect to the other experimental data is lower than the other models (BM, TBC, PDK).

5. Conclusions

This work presents a review of the electron ionization cross section models and an upgrade of the characteristic peak models. The results suggested an excellent validation of the hypotheses of the models and a very good ability to evaluate the peaks of the experimental spectra. Moreover, peak calculation based on the direct radiation depends solely on physical parameters that can be easily obtained from the literature, making it relatively simple to implement.

The only limitation element in our model, which is common to the others in the literature, is the fact that the electron energy loss is modeled using the Continuous Slowing Down Approximation (CSDA) range (Thompson et al., 2009), while the auto-attenuation

of the anode uses the Thomson–Whiddington relation. Further studies have to solve this limitation in order to unify the calculation of the electron penetration and energy loss. Additional researches are necessary to understand the behavior of B_k as a function of Z and a means of estimating the term Q.

The presented model contributes to the field by offering an improved simulation of a realistic x-ray beam emerging from a common diagnostic x-ray tube with a complete and detailed spectrum that lends itself to further studies of added filtration, thus providing an optimized beam for different medical diagnostic applications.

References

Bethe, V.H., 1930. Zur Theorie des Durchgangs schneller Korpuskularstrahlen durch Materie. Ann. Phys. 397 (3), 325–400.

Bhat, M., Pattison, J., 1998. Diagnostic x-ray spectra: a comparison of spectra generated by different computation methods with a measured spectrum. Med. Phys. 25 (1), 114–120.

Birch, R., Marshall, M., 1979. Computation of bremsstrahlung x-ray spectra and comparison with spectra measured with a Ge(Li) detector. Phys. Med. Biol. 24 (3), 505–517.

Bontempi, M., Andreani, L., Rossi, P.L., Visani, A., 2010. Monte Carlo simulator of realistic x-ray beam for diagnostic applications. Med. Phys. 37 (8), 4201–4209.

Casnati, E., Tartari, A., Baraldi, C., 1982. An empirical approach to K-shell ionisation cross section by electrons. J. Phys. B: At. Mol. Phys. 15, 155–167.

Costa, P.R., Nersissian, D.Y., Salvador, F.C., Rio, P.B., Caldas, L.V.E., 2007. Generation of calibrated tungsten target X-ray spectra: modified TBC model. Health Phys. 92 (1), 24–32.

Deutsch, H., Becker, K., Matt, S., Märk, T.D., 2000. Theoretical determination of the absolute electron-impact ionization cross section of molecules. Int. J. Mass Spectrom. (197), 37–69.

Dyson, N., 1990. X-rays in Atomic and Nuclear Physics, 2nd edition. Cambridge University Press, New York, USA.

Fewell, T.R., Shuping, R.E., 1977. Photon energy distribution of some typical diagnostic x-ray beams. Med. Phys. 4 (3), 187–197.

Fewell, T.R., Shuping, R.E., Hawkins, K.R., 1981. Handbook of Computed Tomography X-ray Spectra. DHHS Publication; No. (FDA) 81-8162. Rockville, MD; U.S. Department of Health and Human Services, Public Health Service, FDA, Bureau of Radiological Health, U.S. Government Printing Office, Washongton D.C.

Gan, F., Ruan, G., Mo, J., 2006. Baseline correction by improved iterative polynomial fitting with automatic threshold. Chemom. Intell. Lab. Syst. 82 (1–2), 59–65.

Green, M., Cosslett, V., 1961. The efficiency of production of characteristic X-radiation in thick targets of a pure element. Proc. Phys. Soc. 78 (6), 1206–1214.

Green, M., Cosslett, V., 1968. Measurements of K, L and M shell x-ray production efficiencies. J. Phys. D: Appl. Phys. 1 (4), 425–436.

Gryzinski, M., 1965a. Classical theory of atomic collisions. I. Theory of inelastic collisions. Phys. Rev. 138 (2A), A336–A358.

Gryzinski, M., 1965b. Two-particle collisions. II. Coulomb collisions in the laboratory system of coordinates. Phys. Rev. 138 (2A), A332–A335.

Hombourger, C., 1998. An empirical expression for K-shell ionization cross section by electron impact. J. Phys. B: At. Mol. Opt. Phys. 31, 3693–3702.

Hubbell, J.H., Seltzer, S.M., 1996. Tables of x-ray mass attenuation coefficients and mass energy-absorption coefficients.

Kramers, H.A., 1923. On the theory of x-ray absorption and of the continuous x-ray spectrum. Philos. Mag. 46, 836–871.

Pella, P., Feng, L., Small, J., 1985. An analytical algorithm for calculation of spectral distributions of x-ray tubes for quantitative x-ray fluorescence analysis. X-ray Spectrom. 14 (3), 125–135.

Poludniowski, G.G., 2007. Calculation of x-ray spectra emerging from an x-ray tube. Part II. X-ray production and filtration in x-ray targets. Med. Phys. 34 (6), 2175–2186.

Poludniowski, G.G., Evans, P.M., 2007. Calculation of x-ray spectra emerging from an x-ray tube. Part I. Electron penetration characteristics in x-ray targets. Med. Phys. 34 (6), 2164–2174.

Storm, L., Israel, H.I., 1970. Photon cross sections from 1 keV to 100 MeV for elements $Z=1$ to $Z=100$. At. Data Nucl. Data Tables 7 (6), 565–681.

Talukder, M.R., Bose, S., Takamura, S., 2008. Calculated electron impact K-shell ionization cross section for atoms. Int. J. Mass Spectrom. 269, 118–130.

Tang, C.-H., An, S., Fan, X.-Q., Luo, Z.-M., 2001. An empirical formula of atomic K-shell ionization cross sections by electron impact. Chin. Phys. Lett. 18 (8), 1053–1055.

Thompson, A., Attwood, D., Gullikson, E., Howells, M., Kim, K.-J., Kirz, J., Kortright, J., Lindau, I., Liu, Y., Pianetta, P., Robinson, A., Scofield, J., Underwood, J., Williams, G., Winick, H., 2009. X-ray Databooklet, 3rd edition. Lawrence Livermore National Laboratory, University of California, Berkeley.

Tothill, P., 1968. The ratio of K characteristic to total radiation emitted from a tungsten target x-ray tube. J. Phys. D: Appl. Phys. 1 (2), 1093–1107.

Tucker, D.M., Barnes, G.T., Chakraborty, D.P., 1991. Semiempirical model for generating tungsten target x-ray spectra. Med. Phys. 18 (2), 211–218.

Vignes, A., Dez, G., 1968. Distribution in depth of the primary X-ray emission in anticathodes of titanium and lead. J. Appl. Phys. 1 (2), 1309–1322.